COMMUNICATIONS PHYSICS

ARTICLE

DOI: 10.1038/s42005-018-0068-6 OPEN

Clogging and jamming of colloidal monolayers driven across disordered landscapes

Ralph L. Stoop[1] & Pietro Tierno[1,2,3]

Understanding microscale transport across heterogeneous landscapes is relevant for many phenomena in condensed matter physics, from pinning of vortices in dirty superconductors, to electrons on liquid helium, skyrmions, and active matter. Here, we experimentally investigate the clogging and jamming of field tunable interacting colloids driven through a quenched disordered landscape of fixed obstacles. We focus on the emergent phenomenon of clogging, that has been the matter of much investigation at the level of a single aperture in macroscopic and granular systems. With our colloidal system, we find that quenched disorder significantly alters the particle flow, and we provide the experimental observation of the "Faster is Slower" effect with quenched disorder, that occurs when increasing the particle speed. Further, we show that clogging events may be controlled by tuning the pair interactions during transport, such that the colloidal flow decreases for repulsive interactions, but it increases for anisotropic attraction.

[1] Departament de Física de la Matèria Condensada, Universitat de Barcelona, 08028 Barcelona, Spain. [2] Institut de Nanociència i Nanotecnologia, Universitat de Barcelona, Barcelona 08028, Spain. [3] Universitat de Barcelona Institute of Complex Systems (UBICS), Universitat de Barcelona, Barcelona 08028, Spain. Correspondence and requests for materials should be addressed to P.T. (email: ptierno@ub.edu)

Particle transport through heterogeneous media is a fundamental problem across several disciplines as physics, biology, and engineering. In condensed matter, the inevitable presence of quenched disorder affects the transport properties of several systems, from vortices in high T_c superconductors[1,2], to electrons on the surface of liquid helium[3], skyrmions[4], and active matter[5]. At the macroscopic scale, a disorder in the form of obstacles, wells, or barriers severely alters the flow of bubbles[6,7], granular media[8,9], bacteria[10], sheep[11], or pedestrians[12]. Already a collection of particles that are forced to pass through a small constriction displays a complex dynamics, including flow intermittency, a precursor of blockage via formation of particle bridges and arches. The latter phenomenon is known as clogging, and is responsible for the flow arrest in different technological systems, from microfluidics, or silo discharge, to gas and oil flow through pipelines. Clogging is also directly related to jamming, which occurs when, above a threshold density, a loose collection of elements reaches a solid-like phase with a finite yield[13]. Jammed systems are associated with the existence of a well defined rigid state and a new type of zero-temperature critical point[14,15]. In contrast, the local and spatially heterogeneous nature of clogging makes it more difficult to be characterized and controlled, despite its technological relevance.

In previous experimental realizations, clogging has received much attention at the level of a single bottleneck[16,17], while studies addressing the dynamics of microscale systems driven through heterogeneous landscapes are rather scarce[5]. In contrast, recent theoretical works demonstrated the rich phenomenology of transport and clogging across ordered[18,19] or disordered[20] landscapes. The advantage of using colloidal particles as model systems for clogging is their flexibility, since external fields may be used to create driving forces for transport[21,22], external potentials[23,24], or to tune in situ the pair interactions[25].

Here, we experimentally investigate the flow properties of a monolayer of paramagnetic colloidal particles that is driven across a heterogeneous landscape composed of disordered obstacles. We find that already the presence of few obstacles significantly alters the collective dynamics by creating regions where clogs, intermittent, and free flow coexist. The system mean speed decreases by increasing the density of flowing particles or obstacles. When increasing the particle speed, we find an overall decrease of the mean speed, and this provides an experimental evidence of the "Faster is Slower" effect. Further, we show how to control and reduce the formation of clogs by tuning the pair interactions between the moving colloids. These findings remark the importance of particle speed and interactions on the clogging process.

Result

Magnetic transport of colloidal monolayers. We transport paramagnetic colloidal particles with diameter $d_m = 2.8\,\mu$m by using a magnetic ratchet effect generated at the surface of a uniaxial ferrite garnet film (FGF). The FGF is characterized by a parallel stripe pattern of ferromagnetic domains with alternating up and down magnetization, a spatial periodicity of $\lambda = 2.6\,\mu$m at zero applied field, and a saturation magnetization $M_s = 1.3{\cdot}10^4$ A m^{-1}, Fig. 1a. To introduce quenched disorder in the system, we use silica particles with a diameter $d_o = 5\,\mu$m, larger than the magnetic colloids and thus distinguishable from them. Previous to the experiments, the particles are let sediment on top of the FGF, and irreversibly attached there by screening the electrostatic interactions via the addition of salt. Afterwards, the substrate is dried and the paramagnetic colloids are sedimented above, more details are given in the "Methods" section.

Using this procedure, we generate a random array of obstacles that are evenly distributed across the substrate. The corresponding disorder is spatially uncorrelated and has no detectable features of ordering, as shown by the absence of secondary peaks in the pair correlation functions $g(r)$ of the silica particles, calculated for different samples in Fig. 1b. The transport mechanism was previously introduced for an obstacle-free substrate[26], and here will be briefly described. Above the FGF, the paramagnetic colloids are driven by a rotating magnetic field polarized in the $(\hat{x}, \hat{z})$ plane,

$$\mathbf{H} \equiv [H_x cos(\omega t)\hat{\mathbf{e}}_x - H_z sin(\omega t)\hat{\mathbf{e}}_z] \quad (1)$$

with frequency ω and amplitudes (H_x,H_z). The applied field modulates the stray magnetic field at the FGF surface, and generates a periodic potential that translates at a constant and frequency tunable speed, $v_m = \lambda\omega/(2\pi)$. The potential is capable of transporting the colloidal particles that are trapped in its energy minima, Fig. 1a. As shown in Fig. 1c, by varying the driving frequency, the particles undergo a sharp transition from a phase-locked motion with $\langle v_x\rangle = v_m$ (synchronous regime), to a sliding dynamics (asynchronous regime) resulting from the loss of synchronization with the traveling potential. From the particle speed we can calculate the corresponding Péclet number Pe, as the ratio between the Brownian time τ_B required by the particle to diffuse its own radius, and the driven time τ_D required to move its radius due to the magnetic landscape. Here, $\tau_B = d_m^2/(4D_{eff})$, being $D_{eff} = 0.14\,\mu$m^2 s^{-1} the effective diffusion coefficient of the paramagnetic colloid, as measured from the mean square displacement[27], and $\tau_D = d_m/(2\langle v_x\rangle)$. Thus for the synchronous regime in the obstacle-free case we have $\langle v_x\rangle \in [2, 23.5]\,\mu$m s^{-1} which corresponds to $Pe \in [20, 235]$. Throughout this work, we restrict the angular frequency to the former regime, and vary ω to tune the particle speed. Given the strong magnetic attraction of the FGF, the particle motion is essentially two-dimensional, with negligible out-of-plane thermal fluctuations. Further, the ratio between the field amplitudes H_x/H_z will be used to tune the pair interactions. Unless stated otherwise, we initially set this ratio to $H_x/H_z \sim 0.7$ such to minimize these interactions and obtain an hard-sphere-like behavior.

Particle transport across disordered landscapes. Figure 1d shows two experimental images of a dense collection of paramagnetic colloids driven against $N = 80$ silica particles. From the trajectories, it emerges that the magnetic colloids surpass the silica particles by following a path similar to laminar flow. We use an upright microscope equipped with a charge-coupled device camera, to record real-time videos of the system dynamics, and analyze different subsets of a total field of view of $145 \times 108\,\mu$m^2. We then determine the positions $(x_i(t), y_i(t))$ of each magnetic colloid $i = 1\ldots N$ via particle tracking routines[28], and measure the instantaneous velocity $v_x(t) = \frac{1}{N}\sum_i \frac{dx_i}{dt}$, and its mean value $\langle v_x(t)\rangle$, with the time-average taken in the stationary regime.

We start by analyzing the collective dynamics across the disordered landscape by varying the area fractions of magnetic colloids, Φ_m and obstacles, Φ_o. Here, $\Phi_j = N_j\pi(d_j/2)^2/A_o$, being N_j the number of elements j having diameter d_j and located in the area A_0 . In Fig. 2a, we show the time evolution of the instantaneous velocity averaged over all particles in the system, and measured parallel $(v_x(t))$ and perpendicular $(v_y(t))$ to the direction of motion. The area fraction of magnetic particles used is $\Phi_m = 0.4$ and obstacle $\Phi_o = 0.1$, thus well inside the "abnormal flow" regime of the phase diagram in Fig. 2b. We find that after a relatively short transient time τ, the system settles to a stationary regime where the velocity does not change around its mean value, $\langle v_x\rangle = 6.74 \pm 0.04\,\mu$m s^{-1}. This time can be calculated by fitting the data with an exponential law, $v_x(t) = Aexp(-t/\tau) + \langle v_x\rangle$,

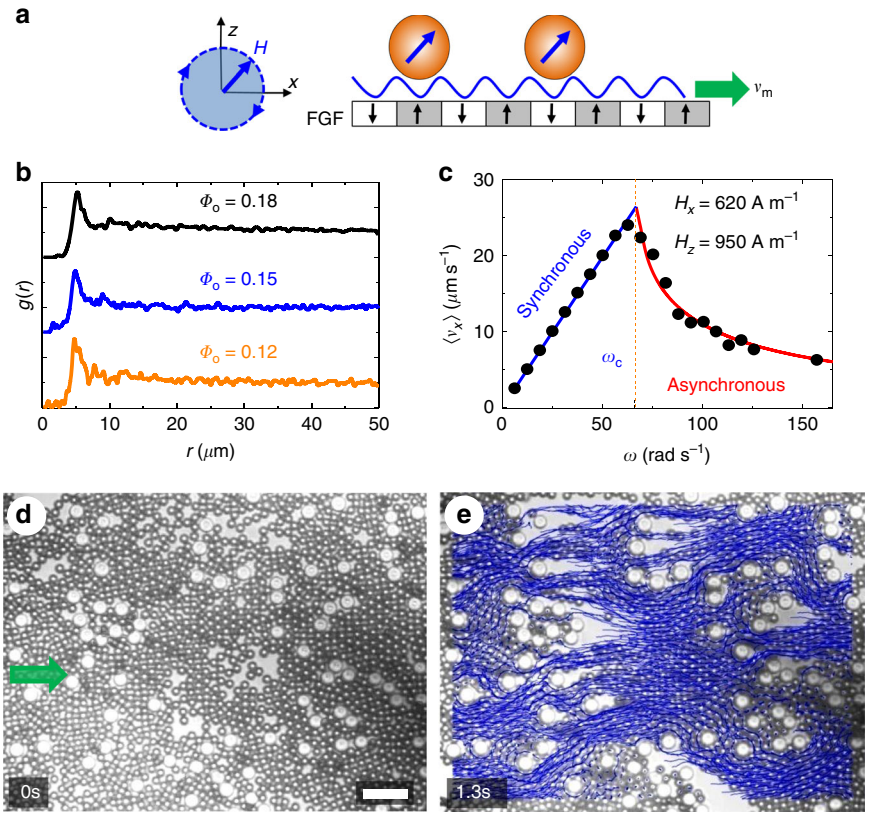

Fig. 1 The disordered landscape and the driven monolayer. **a** Schematic of the traveling wave potential generated at the surface of the ferrite garnet film when subjected to a rotating magnetic field. **b** Pair correlation function $g(r)$ of the silica particles for 3 samples with different obstacle density Φ_O. For clarity the $g(r)$ are rescaled along the $\hat{y}$ axis. **c** Mean particle speed $\langle v_x \rangle$ versus driving frequency ω in the obstacle-free case. Blue [red] fit to the data indicates the synchronous, $\langle v_x \rangle = v_m$ [asynchronous, $\langle v_x \rangle = v_m(1 - \sqrt{1-(\omega_c/\omega)^2})$] regime, being $\omega_c = 68.8$ rad s^{-1} the critical frequency. **d**, **e** Experimental images of a monolayer of paramagnetic colloids (black circles) driven through a disordered landscape of silica particles (white circles) towards right ($\hat{x}$>0). The particle trajectories are superimposed in blue on the image in (**e**) ($t = 1.3$s). The applied field has $\omega = 37.7$ rad s^{-1} and thus $v_m = 15.6$ μm s^{-1} . Scale bar is 20 μm, see also Supplementary movie 1

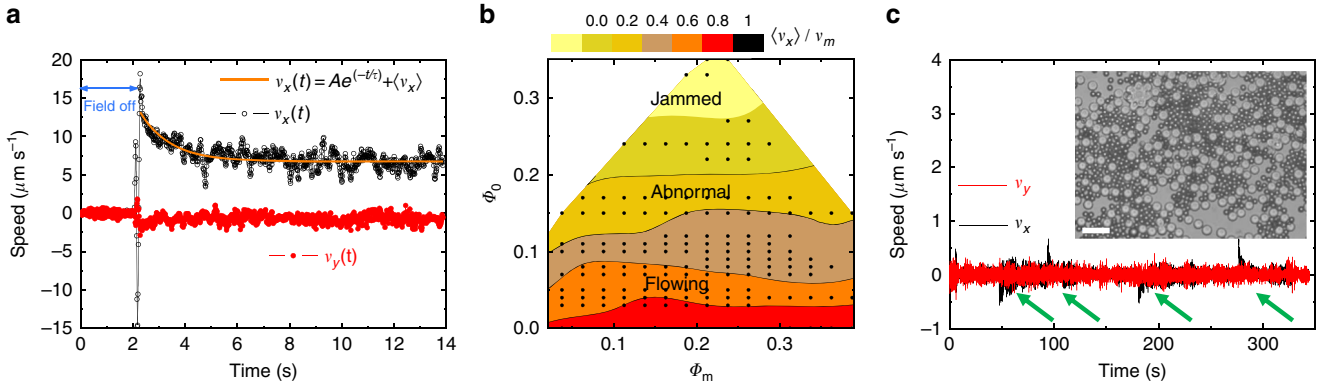

Fig. 2 Particle speed and disorder diagram. **a** Particle speed parallel (v_x, black empty circles) and perpendicular (v_y, red filled circles) to the transport direction ($\hat{x}$). The time of application of the magnetic field corresponds to $t = 2.1$ s. The measurements correspond to an applied field with frequency $\omega = 37.7$ rad s^{-1} ($Pe = 156$). **b** Diagram in the (Φ_m,Φ_o) plane illustrating regions of normal flow ($\langle v_x \rangle / v_m$>0.8), abnormal flow characterized by the coexistence of clogs and flowing particles ($\langle v_x \rangle / v_m \lesssim 0.8$), and jamming that was found above $\Phi_o \sim 0.25$. The magnetic particles are driven in the synchronous regime with $\omega = 37.7$ rad s^{-1}, points are experimental data. **c** Particle speed versus time parallel (v_x, black line) and perpendicular (v_y, red line) to the transport direction ($\hat{x}$) for different reversals of the applied field. These reversals appear as spikes in v_x, and correspond to short rearrangements of few particles within the silica cages. The spikes are indicated by the green arrows. The inset shows an experimental image of a dense array of silica particles $\Phi_o = 0.3$ that entrap the paramagnetic colloids $\Phi_m = 0.25$, scale bar is 20 μm. See also Supplementary movie 2

that allows finding $\tau = 1.16 \pm 0.06$s. In contrast, the mean speed along the perpendicular direction vanishes, $\langle v_y \rangle = 0$, while its fluctuations slightly increase as compared to the zero field case ($t < 2.1$ s). Thus, we use this procedure to find the normalized speed for different experiments by varying the area fraction of particles and obstacles. From the experimental data in Fig. 2a, we find that the initial speed is $v_0 = 0.84 v_m$, with $v_m = 15.6\ \mu\text{m s}^{-1}$ ($Pe = 156$) being the obstacle-free speed. The small difference results from the presence of the silica obstacles. Further, the stationary speed is $\langle v_x \rangle = 0.41 v_m$, and thus less than half of the velocity of the obstacle-free case. In Fig. 2b, we show the different dynamic phases in the (Φ_m, Φ_o) plane in terms of the normalized mean speed, $\langle v_x \rangle / v_m \in [0, 1]$. One could expect a monotonous decrease of the particle mean speed for increasing magnetic particles and obstacle densities. Indeed, the particle flow is maximal at low obstacle density, $\Phi_o < 0.07$, where few silica particles are unable to substantially alter the motion of the magnetic colloids. However, we find a decrease of the mean speed on the left, lower corner of the diagram, at low magnetic particle density, $\Phi_m < 0.1$. This result is appealing since in this regime, the magnetic particles are unlikely to hamper each other via the formation of clogs and therefore a high speed, similar to the case of obstacle-free, is expected. However, at such low magnetic particle densities, the overall speed is affected by individual particles that are trapped in front of an obstacle. The trapping occurs when particles hit the obstacle at a small angle of incidence and therefore are not scattered, but rather stop their movement as long as other particles do not release them via collision. For an increased magnetic particle density, these collisions become more frequent, a tendency that decreases the fraction of trapped particles and increases the mean speed. A similar feature has been observed recently via numerical simulations of driven disks across a disorder landscape[29].

Increasing Φ_o reduces the system mean speed, as now flowing and clogged regions coexist. The latter states however, may be easily unclogged by inverting the particle flux, that corresponds to reversing the sense of rotation of the applied field, $H_x \leftrightarrow -H_x$, see below. This extended region of "abnormal flow" includes also cases where the system was almost completely arrested $\langle v_x \rangle / v_m \sim 0.3$, but it could be again fluidized by reversing the applied field. For intermediate Φ_o, we find that at low (high) Φ_m, trapping (clogging) dominate, leading to a highly non-linear dependence of the mean speed on the magnetic particle density. The maximum speed is achieved at low Φ_o and is almost independent on Φ_m since the influence of trapping and clogging are observed to be minimal.

At larger obstacle density, $\Phi_o > 0.25$, the silica particles percolate through the system and surround the magnetic colloids, thus impeding any net movement. This situation is illustrated in Fig. 2c, where the system mean speed goes immediately to zero, $\langle v_x \rangle = 0$ independently on the sense of the applied field, and without any transitory state. Here, the area fraction of the silica obstacles used to jam is $\Phi_o = 0.3$ and the system forms a solid-like phase that cannot be refluidized by the applied drive. We note that in our system we never observe fully clogged states where the mean speed vanishes after a transitory period, and that can be refluidized by inverting the particle current. We did not explore the high density case of magnetic colloids, $\Phi_m > 0.4$, as there we found that pressure from the driven particles favors particle jumping across the obstacles leaving the two-dimensional confinement. In contrast, we observe that the presence of few obstacles strongly reduces the jamming threshold where $\langle v_x \rangle = 0$. In absence of silica particles, the driven colloids will jam near the close packing density, $\Phi_m = \pi/2\sqrt{3} \sim 0.9$. However, a small concentration of obstacles $\Phi_o = 0.25$ reduces the jamming threshold to $\Phi_m = 0.3$. We note that the lack of more data in the diagram at high obstacle density is due to technical difficulty in realizing uniform distributions of obstacles above $\Phi_o \sim 0.25$. At high density, the silica particles were found to frequently form heterogeneous clusters or even 3D aggregates, that make the analysis of the experimental data difficult.

In order to emphasize the fundamental difference between jamming and clogging on a disordered landscape, we show the effect of inverting the sense of rotation of the magnetic field on the clogging process in Fig. 3a, b. The images at the top illustrate different clusters of magnetic particles that are formed depending on whether the particle flux occurs from left to right, (top images 1, 3, 5) or from right to left (top images 2, 4). The magnetic field is inverted by changing the polarity of one of the two components of the applied field, here $H_x \leftrightarrow -H_x$. Inverting the particle flux alters the system transport properties, and we find a different normalized mean speed in the two cases, $\langle v_x \rangle / v_m = 0.33$ when the particles are driven towards right, $\langle v_x \rangle / v_m = 0.48$ when driven towards left. The mean velocities are similar when the particles are driven along the same direction but starting at different times.

Observation of the "Faster is Slower" effect. In Fig. 4a, b, we investigate the effect of varying the particle speed via the driving frequency ω, and keeping a constant concentration of $\Phi_m = 0.25$. We experimentally observe the "Faster is Slower" (FIS) effect, where the mean speed of the system $\langle v_x \rangle$ strongly decreases as ω

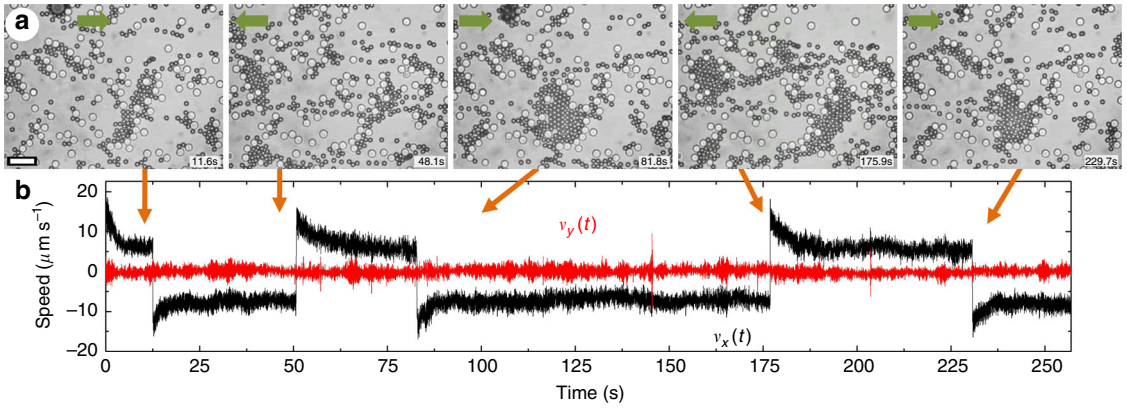

Fig. 3 Effect of driving direction on clogging. **a** Series of experimental snapshots of an ensemble of paramagnetic colloids driven against a disordered array of silica obstacles. The arrows at the top indicate the direction of the particle motion. Scale bar is 20 μm. **b** Particle speed parallel (v_x, black line) and perpendicular (v_y, red line) to the transport direction ($\hat{x}$). Each time the sense of rotation of the applied field is inverted $H_x \leftrightarrow -H_x$, the speed changes sign displaying a jump. See Supplementary movie 3

increases above $\Phi_o = 0.03$. The FIS effect was originally observed when simulating the dynamics of pedestrians trying to escape through a narrow exit[30]. A recent surge of interest on FIS[31] resulted from the possibility to observe a similar effect in other systems[32], although its investigation has been always limited to a single constriction. On a collective level, the effect of the velocity drop by an increase of the applied driving force has been reported by different theoretical works in condensed matter systems[33–37], although with scarce experimental evidence. Here, when considering a heterogeneous landscape, we find that FIS is greatly enhanced by the disorder. Already a small area fraction $\Phi_o = 0.08$, is able to reduce the speed of a ~45% with respect to the free case when increasing the driving frequency from 6.3 to 50.3 rad s^{-1}, as shown by the magenta curve in Fig. 4. We have also performed few experiments to investigate the dynamics across an individual constriction composed of a pair of silica particles separated by a surface to surface distance $d \geq 3$ μm in a cluster of connected obstacles. In general, we find an intermittent flow of the magnetic colloids with an exponential distribution of burst size, as already reported in numerical simulations of flowing colloids[38]. Further, these preliminary results indicate that the Faster is Slower effect is absent (or largely suppressed) at the level of a single constriction, while it emerges on a disordered landscape due to the complex interplay of multiple large clogs that form across the film.

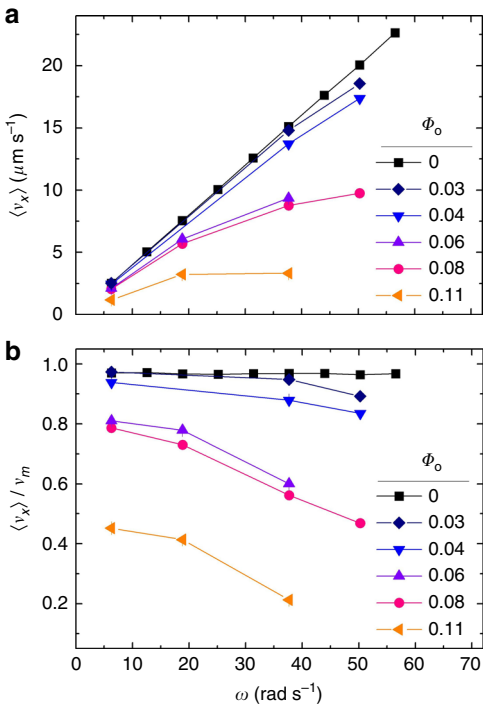

Fig. 4 "Faster is Slower" effect on a disordered landscape. **a** Mean speed $\langle v_x \rangle$ and **b** normalized speed $\langle v_x \rangle / v_m$ versus driving frequency ω for different disorder densities Φ_o. All data in (**a**) and (**b**) were taken for $H_x = 0.048 M_s$, $H_z = 0.073 M_s$, after averaging over a long time in the stationary regime, starting from times $t > \tau$

Discussion

Our system further allows to tune the pair interactions between the moving colloids by varying the in-plane field component, H_x. Above the magnetically modulated FGF, the effective interaction potential between two paramagnetic colloids can be calculated via a time average[39]. In polar coordinates (r, ϑ) this potential is given by $U_{dd} = \alpha[H_x^2(1 + 3cos2\vartheta) - 2H_z^2]/r^3$, where $\alpha = \chi d_m^3/(96\lambda^3 M_s^2)$ and $\chi = 0.4$ is the effective volume susceptibility of the particles. For the field strengths employed here, $H_{x,z} \in [0.02, 0.15] M_s$, the magnetic dipolar interactions between two particles at a distance d_m are of the order $U_d \in [2, 95] k_B T$, thus higher than other interactions as electrostatic or thermal ones. Thus, at a fixed value of H_z, the sign of the pair interaction is repulsive when $H_x < H_z/\sqrt{3\,cos^2\,\vartheta - 1}$, and attractive otherwise. Further, the dipolar interactions between two colloids are strongly anisotropic, Fig. 5a, b. We consider two representative cases characterized by a complete repulsion for $H_x = 0.4 H_z$, and attraction (repulsion), for $H_x = 1.8 H_z$ when the relative angle ϑ between the particles lies in the region $\vartheta \in [n\pi - \vartheta_m, n\pi + \vartheta_m]$ (otherwise). Here $n = 0,1\ldots$ and $\vartheta_m = 48.7^o$. The corresponding average particle velocities parallel ($\langle v_x \rangle$) and normal ($\langle v_y \rangle$) to the direction of motion are shown in Fig. 5c. We find that the attractive interactions, combined with repulsion at large ϑ, facilitate the formation of parallel trains of magnetic colloids that are able to easily move across the disorder landscape. These trains slide plastically through the obstacles and, as a result, the amplitude of fluctuations along the normal direction increases, being the variance $\delta v_y = 1.15$ μm s^{-1} for the attractive case, the double than in the repulsive case ($\delta v_y = 0.54$ μm s^{-1}). This situation may appear as counter intuitive, since one mechanism of clogging in microchannels is the aggregation of attractive particles at the entrance[7]. However, the anisotropic nature of dipolar interactions facilitates the system fluidization, as it induces the formation of elongated flexible structures. When a chain hits an obstacle, the composing particles can laterally buckle and return back to their position in order to surpass it. The elastic force of these particles can be derived by considering the lateral displacements h in a chain of N equispaced colloids and interacting via the usual dipolar potential between the magnetic moments $m_i = \pi d_m^3 \chi H_x/6$ induced by the in-plane component H_x, $U_d = \beta(1 - 3\,cos^2\,\theta)/r^3$. Here, $\beta = \mu_m m^2/(4\pi)$, μ_m the medium permeability, and θ the angle that the dipoles form with the line. At the nearest neighbor level and performing a Taylor expansion around this line, the lateral component of the force is $F_y = 6\beta(h_{i+1} - 2h_i + h_{i-1})/d_m^2$, being h_i the distance from the line of particle i. At high amplitudes $H_x > 0.3 M_s$, the chains become stiffer and this reduces the lateral mobility of the particles decreasing the unclogging effect. In Fig. 5d, we report the effect of varying the pair interaction at different disorder densities, including the extreme cases of free-flow ($\Phi_0 = 0$) and completely clogged states ($\Phi_0 = 0.42$). The velocity dependence on H_x can be described by an exponential growth, $\langle v_x \rangle = (\langle v_0 \rangle - \langle v_\infty \rangle)(1 - exp(-H_x/H_c)) + \langle v_0 \rangle$, being $H_c = H_z/\sqrt{2}$ (red arrow in Fig. 5d), v_0 and v_∞ the limit velocities acquired for very small and large H_x, respectively. As shown in the inset of Fig. 5d, by fitting to the data we obtain a linear but different decrease of both quantities with Φ_o, implying the presence of different competing effects. For the repulsive case ($H_x < H_c$), the average field induces dipoles that are perpendicular to the FGF plane, forcing the clusters of magnetic particles to expand and increasing the inter-particle distance d_m, and thus effective Φ_m. This also corresponds to a global hardening of the colloidal monolayer as now the particles are less prone to be displaced from their lattice position. In addition, the increase of d_m reduces the effect of the hydrodynamic lubrication forces that act on very short inter-surface distances. The particles thus easily form clogs that are more difficult to be refluidized, and the system velocity rapidly drops. In contrast, for anisotropic attraction the rise of the velocity is slower since, even if chain flexibility reduces the clogging probability, the formed colloidal trains repel each other, and this effect produces again a smaller rise in the area fraction of the driven colloids.

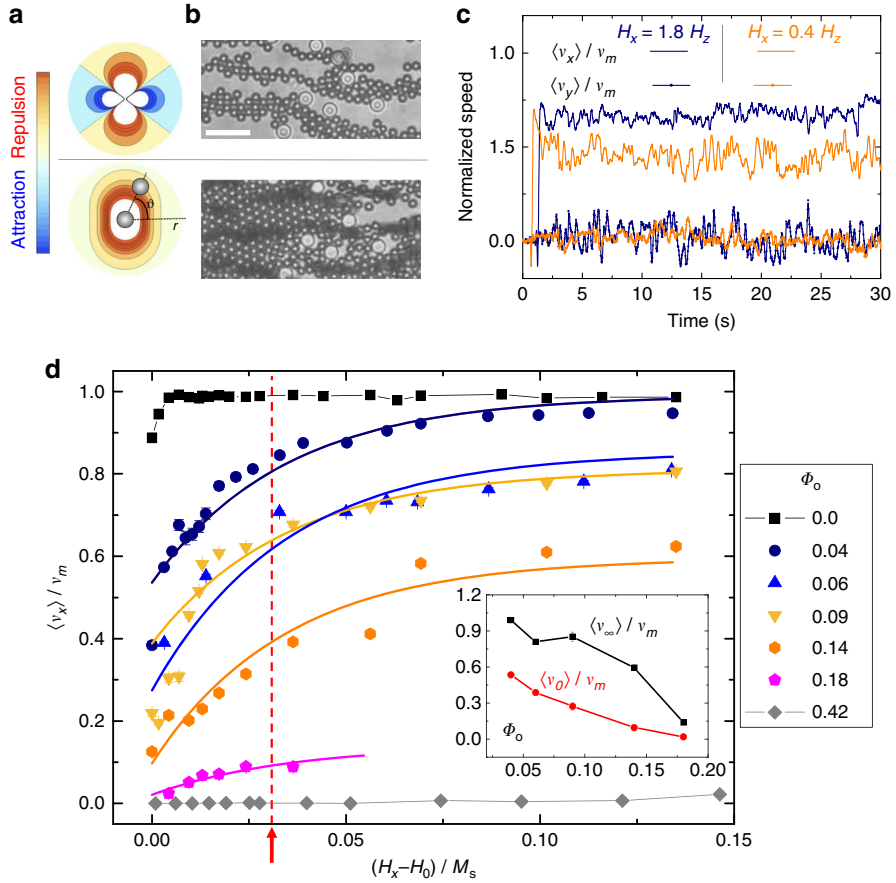

Fig. 5 System fluidification via pair interactions. **a** Polar plots of the dipolar interactions between two paramagnetic colloids for $H_x = 1.8H_z$ (top) and $H_x = 0.4\,H_z$ (bottom), with $H_z = 0.073M_s$. Red (blue) region denotes repulsion (attraction). **b** Experimental snapshots of the corresponding situations ($\omega = 37.7$ rad s^{-1}, $\Phi_m = 0.3$, $\Phi_o = 0.06$), scale bar is 20 μm, see Supplementary movie 4. **c** Averaged velocities $(\langle v_x \rangle, \langle v_y \rangle)$ for the two cases. **d** $\langle v_x \rangle / v_m$ versus H_x, at different disorder densities Φ_o ($\Phi_m = 0.3$). Continuous lines are exponential fits, the red arrow denotes H_c, $H_0 = 0.017M_s$. The inset shows the resulting v_0, v_∞ versus Φ_o

To conclude, we studied the clogging process in a system composed of interacting paramagnetic colloids driven across a quenched disorder landscape. We demonstrate the emergence of the FIS effect due to quenched disorder. We also investigate the role of the pair interactions on the collective transport and how flexibility and directionality facilitate unjamming. Even though the experiments are based on the magnetic manipulation of domain walls in a FGF film, the observed phenomena are common to many other interacting driven systems in presence of quench disorder at the microscale.

Methods

Experimental procedures. The FGF of wavelength $\lambda = 2.6$ μm and saturation magnetization $M_s = 1.3{\cdot}10^4$ A /m was grown by dipping liquid phase epitaxy on a gadolinium gallium garnet substrate. To prevent adhesion of the paramagnetic colloidal particles on the substrate, before the experiments, the FGF is coated with a 1 μm-thick layer of a photoresist (AZ-1512 Microchem, Newton, MA) by using spin coating and backing procedures. Before each measurement, the FGF is rinsed in highly deionized water (MilliQ, Millipore).

Disorder realization. Quenched disorder is introduced by the deposition of silica dioxide particles (44054-5ML-F, Sigma-Aldrich) of diameter $d_o = 5$ μm and standard deviation $\sigma \leq 0.35$ μm. The particles are diluted in highly deionized water at different concentrations and a droplet of the solution is placed on top of the FGF surface. After a short equilibration time of 1–2 min, the particles sediment above the FGF surface, while their negative surface charge prevents particle sticking on the substrate. The silica particles are immobilized by adding a solution composed of a highly deionized water and 10 mM NaCl salt. The ions of the salt screen the electrostatic double layer favoring permanent linkage of the silica particle to the FGF via attractive van der Waals interactions. After leaving the system to equilibrate for few minutes, we remove the solution by using a pipette and immediately replace the medium by a water dispersion containing the paramagnetic colloidal particles. These are monodisperse paramagnetic colloids (Dynabeads M-270, Dynal) of diameter $d_m = 2.8$ μm and effective magnetic volume susceptibility $\chi = 0.4$. The particles are composed of a polystyrene matrix with surface carboxylic groups, and doped (~20% by weight) with superparamagnetic iron-oxide grains.

Experimental setup. Rotating magnetic fields in the $(\hat{x}, \hat{z})$ plane are applied via custom-made Helmholtz coils connected to two independent power amplifiers (AMP-1800, Akiyama) controlled by a wave generator (TGA1244, TTi). Particle positions and dynamics are recorded by using an upright optical microscope (Eclipse Ni, Nikon) equipped with a 100 × 1.3 NA oil immersion objective and a charge-coupled device camera (Scout scA640-74fc, Basler) working at 75 frames per second. By adding a 0.45× TV adapter to the optical path, we obtain a total field of view of 145 × 109 μm. For all measurements of Figs. 4 and 5 of the main text, a subset of $A_o = 77 \times 77$ μm is selected and used for the analysis.

Data availability

The data that support the findings of this study are available from the corresponding author upon request.

Received: 7 June 2018 Accepted: 25 September 2018
Published online: 25 October 2018

References

1. Bhattacharya, S. & Higgins, M. J. Dynamics of a disordered flux line lattice. *Phys. Rev. Lett.* **70**, 2617–2620 (1993).

2. Blatter, G., Feigel'man, M. V., Geshkenbein, V. B., Larkin, A. I. & Vinokur, V. M. Vortices in high-temperature superconductors. *Rev. Mod. Phys.* **66**, 1125–1388 (1994).
3. Rees, D. G., Totsuji, H. & Kono, K. Commensurability-dependent transport of a Wigner crystal in a nanoconstriction. *Phys. Rev. Lett.* **108**, 176801 (2012).
4. Reichhardt, C., Ray, D. & Reichhardt, C. J. O. Collective transport properties of driven skyrmions with random disorder. *Phys. Rev. Lett.* **114**, 217202 (2015).
5. Morin, A., Desreumaux, N., Caussin, J.-B. & Bartolo, D. Distortion and destruction of colloidal flocks in disordered environments. *Nat. Phys.* **13**, 63 (2017).
6. Champagne, N., Vasseur, R., Montourcy, A. & Bartolo, D. Traffic jams and intermittent flows in microfluidic networks. *Phys. Rev. Lett.* **105**, 044502 (2010).
7. Dressaire, E. & Sauret, A. Clogging of microfluidic systems. *Soft Matter* **13**, 37–48 (2017).
8. Bideau, D. & Hansen, A. *Disorder and Granular Media*. Elsevier Science Publishers: North-Holland, 1993.
9. To, K., Lai, P.-Y. & Pak, H. K. Jamming of granular flow in a two-dimensional hopper. *Phys. Rev. Lett.* **86**, 71–74 (2001).
10. Sendekie, Z. B., Gaveau, A., Lammertink, R. G. H. & Bacchin, P. Bacteria delay the jamming of particles at microchannel bottlenecks. *Sci. Rep.* **6**, 31471 (2016).
11. Garcimartn, A. et al. Flow and clogging of a sheep herd passing through a bottleneck. *Phys. Rev. E* **91**, 022808 (2015).
12. Yanagisawa, D. et al. Introduction of frictional and turning function for pedestrian outflow with an obstacle. *Phys. Rev. E* **80**, 036110 (2009).
13. Cates, M. E., Wittmer, J. P., Bouchaud, J.-P. & Claudin, P. Jamming, force chains, and fragile matter. *Phys. Rev. Lett.* **81**, 1841–1844 (1998).
14. Liu, A. J. & Nagel, S. R. Jamming is not just cool anymore. *Nature* **396**, 21 (1998).
15. Goodrich, C. P., Liu, A. J. & Sethna, J. P. Scaling ansatz for the jamming transition. *Proc. Natl Acad. Sci. USA* **113**, 97451 (2016).
16. Haw, M. D. Jamming, two-fluid behavior, and "self-filtration" in concentrated particulate suspensions. *Phys. Rev. Lett.* **92**, 185506 (2004).
17. Zuriguel, I. Invited review: clogging of granular materials in bottlenecks. *Pap. Phys.* **6**, 060014 (2014).
18. Reichhardt, C. & Olson Reichhardt, C. J. Active matter transport and jamming on disordered landscapes. *Phys. Rev. E* **90**, 012701 (2014).
19. Yang, Y., McDermott, D., Reichhardt, C. J., Olson & Reichhardt, C. Dynamic phases, clustering, and chain formation for driven disk systems in the presence of quenched disorder. *Phys. Rev. E* **95**, 042902 (2017).
20. Glanz, T., Wittkowski, R. & Löwen, H. Symmetry breaking in clogging for oppositely driven particles. *Phys. Rev. E* **94**, 052606 (2016).
21. Tierno, P., Sagués, F., Johansen, T. H. & Fischer, T. M. Colloidal transport on magnetic garnet films. *Phys. Chem. Chem. Phys.* **11**, 9615–9625 (2009).
22. Dobnikar, J., Snezhko, A. & Yethiraj, A. Emergent colloidal dynamics in electromagnetic fields. *Soft Matter* **9**, 3693–3704 (2013).
23. Löwen, H. Colloidal dispersions in external fields: recent developments. *J. Phys. Condens. Matter* **20**, 404201 (2008).
24. Bohlein, T., Mikhael, J. & Bechinger, C. Observation of kinks and antikinks in colloidal monolayers driven across ordered surfaces. *Nat. Mater.* **11**, 126130 (2012).
25. Bharti, B., Kogler, F., Hall, C. K., Klapp, S. H. L. & Velev, O. D. Multidirectional colloidal assembly in concurrent electric and magnetic fields. *Soft Matter* **12**, 7747–7758 (2016).
26. Tierno, P. Depinning and collective dynamics of magnetically driven colloidal monolayers. *Phys. Rev. Lett.* **109**, 198304 (2012).
27. Tierno, P., Muruganathan, R. & Fischer, T. M. Viscoelasticity of dynamically self-assembled paramagnetic colloidal clusters. *Phys. Rev. Lett.* **98**, 028301 (2007).
28. Crocker, J. C. & Grier, D. G. Methods of digital video microscopy for colloidal studies. *J. Colloid Interface Sci.* **179**, 298 (1996).
29. Peter, H., Libal, A., Reichhardt, C. & Reichhardt, C. J. O. Crossover from jamming to clogging behaviors in heterogeneous environments. *Sci. Rep.* **8**, 2045–2322 (2018).
30. Sticco, I. M., Cornes, F. E., Frank, G. A., Dorso, C. O. & Mouritsen, O. G. Beyond the faster-is-slower effect. *Phys. Rev. E* **96**, 052303 (2017).
31. Helbing, D., Farkas, I. J. & Vicsek, T. Simulating dynamical features of escape panic. *Nature* **407**, 487 (2000).
32. Pastor, J. M. et al. Experimental proof of faster-is-slower in systems of frictional particles flowing through constrictions. *Phys. Rev. E* **92**, 062817 (2015).
33. Zia, R. K. P., Praestgaard, E. L. & Mouritsen, O. G. Getting more from pushing less: negative specific heat and conductivity in nonequilibrium steady states. *Am. J. Phys.* **70**, 384 (2002).
34. Jack, R. L., Kelsey, D., Garrahan, J. P. & Chandler, D. Negative differential mobility of weakly driven particles in models of glass formers. *Phys. Rev. E* **78**, 011506 (2008).
35. Baiesi, M., Stella, A. L. & Vanderzande, C. Role of trapping and crowding as sources of negative differential mobility. *Phys. Rev. E* **92**, 042121 (2015).
36. Bénichou, O., Illien, P., Oshanin, G., Sarracino, A. & Voituriez, R. Nonlinear response and emerging nonequilibrium microstructures for biased diffusion in confined crowded environments. *Phys. Rev. E* **93**, 032128 (2016).
37. Reichhardt, C. & Reichhardt, C. J. O. Negative differential mobility and trapping in active matter systems. *J. Phys. Condens. Matter* **30**, 015404 (2018).
38. Zuriguel, I. et al. Clogging transition of many-particle systems flowing through bottlenecks. *Sci. Rep.* **4**, 7324 (2014).
39. Straube, A. V. & Tierno, P. Tunable interactions between paramagnetic colloidal particles driven in a modulated ratchet potential. *Soft Matter* **10**, 3915 (2014).

Acknowledgements

We thank Tom H. Johansen for the FGF film; H. Massana-Cid and F. Martinez-Pedrero for initial experiments; I. Zuriguel, H. Löwen, and C. Reichhardt for stimulating/inspiring discussions. R.L.S. acknowledges support from the Swiss National Science Foundation (Grant No. 172065). P.T. acknowledges support from the ERC starting grant "DynaMO" (335040) and from MINECO (FIS2016-78507-C2) and DURSI (2014SGR878).

Author contributions

P.T. supervised the work and wrote the paper. R.L.S. performed the experiments and analyzed the data. Both authors discussed and interpreted the results.

Additional information

Supplementary information accompanies this paper at https://doi.org/10.1038/s42005-018-0068-6.

Competing interests: The authors declare no competing interests.

Reprints and permission information is available online at http://npg.nature.com/reprintsandpermissions/

Publisher's note: Springer Nature remains neutral with regard to jurisdictional claims in published maps and institutional affiliations.